Hybrid Membrane-Camouflaged CuS Nanoplatform for Synergistic Nanotherapy of Ovarian Cancer via Chemodynamic and Sonodynamic Effects

*Yuxin Jiang [a, #], Runzi Guo [b, c, d, #], Zhaojun Cui [b, c, d, #], Hongtao Hu[a], Lin Yuan[a], Xun Xu [a], Lin Lin [e, *], Xiuhui Wang [b, c, *], Wenjun Cheng [a, *]*

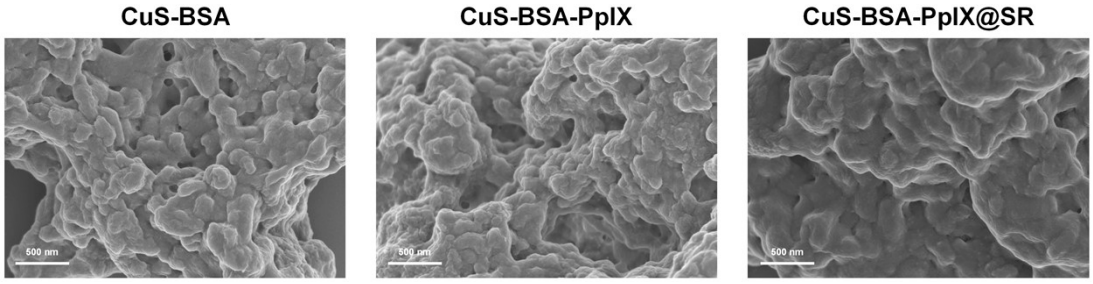

Figure S1. SEM images of CuS, CuS-BSA-PpIX, and CuS-BSA-PpIX@SR nanoparticles.

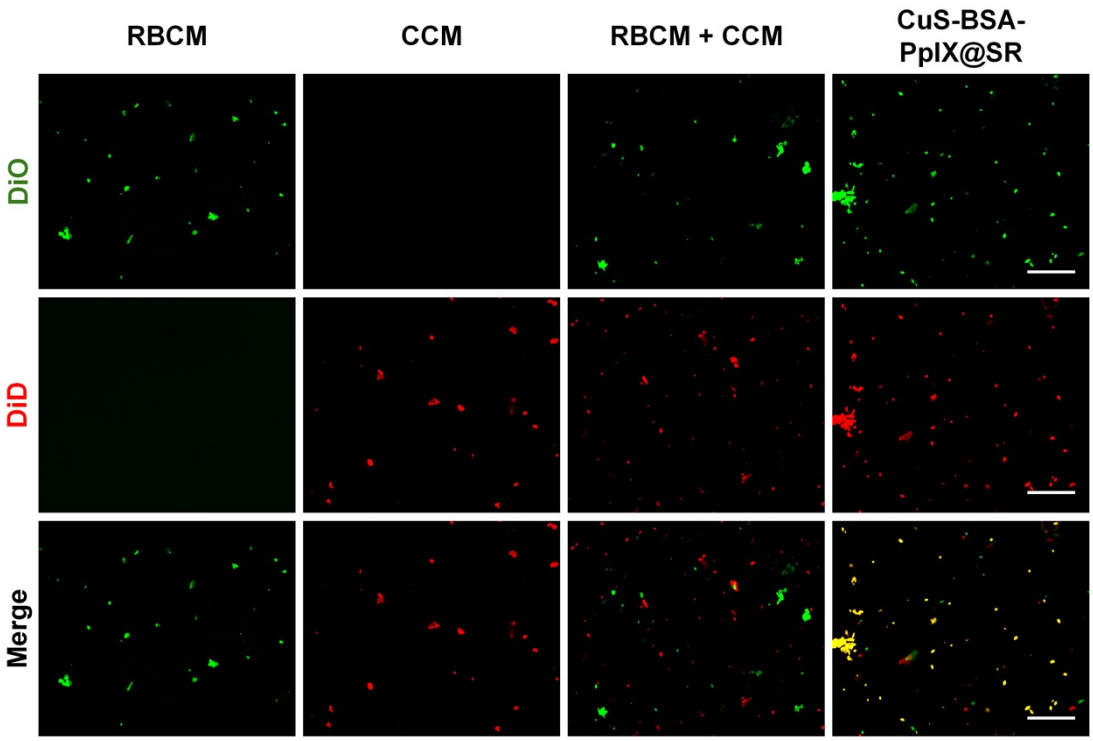

Figure S2. Fluorescent microscopy images of CuS-BSA-PpIX@SR (green = CCM, red = RBCM, brilliant yellow = merge) (Scale bar: 500 μm).

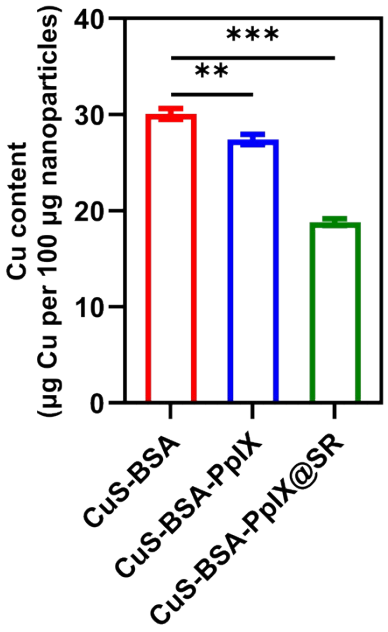

Figure S3. Analysis of Cu content in different nanoparticles (unit: μg Cu per 100 μg nanoparticles). Data are presented as mean ± SD (n = 3). Statistical analysis: one-way ANOVA, Tukey's multiple comparisons test. Significance differences are indicated as $^{**}p<0.01$ and $^{***}p<0.001$, respectively.

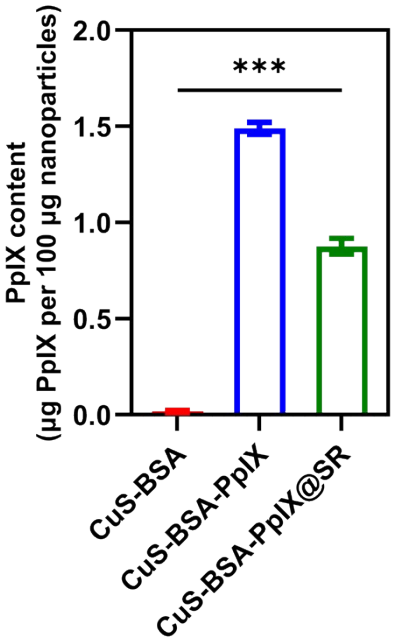

Figure S4. Analysis of PpIX content in different nanoparticles (unit: μg PpIX per 100 μg nanoparticles). Data are presented as mean ± SD (n = 3). Statistical analysis: one-way ANOVA, Tukey's multiple comparisons test. Significance differences are indicated as $^{***}p<0.001$, respectively.

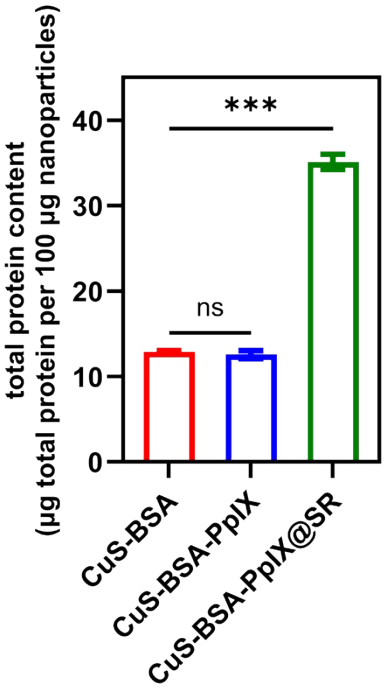

Figure S5. Analysis of total protein content in different nanoparticles (unit: μg total protein per 100 μg nanoparticles). Data are presented as mean ± SD (n = 3). Statistical analysis: one-way ANOVA, Tukey's multiple comparisons test. Significance differences are indicated as ns and ***p<0.001, respectively.

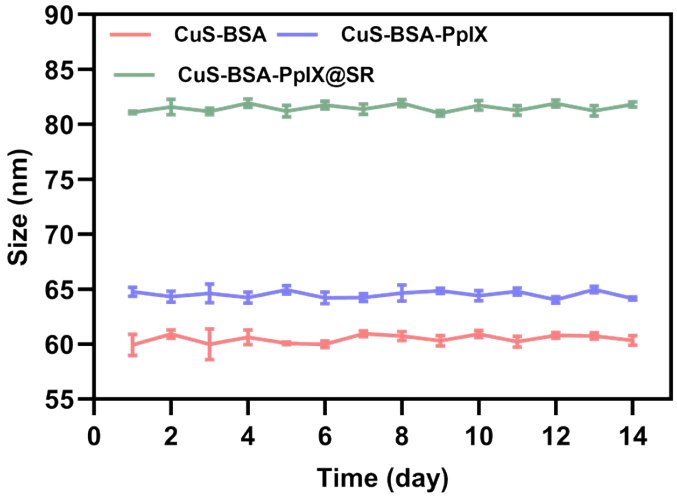

Figure S6. Hydrodynamic size stability analysis of CuS-BSA, CuS-BSA-PpIX and CuS-BSA-PpIX@SR after incubation in PBS for 14 days. Data are presented as mean ± SD (n = 3).

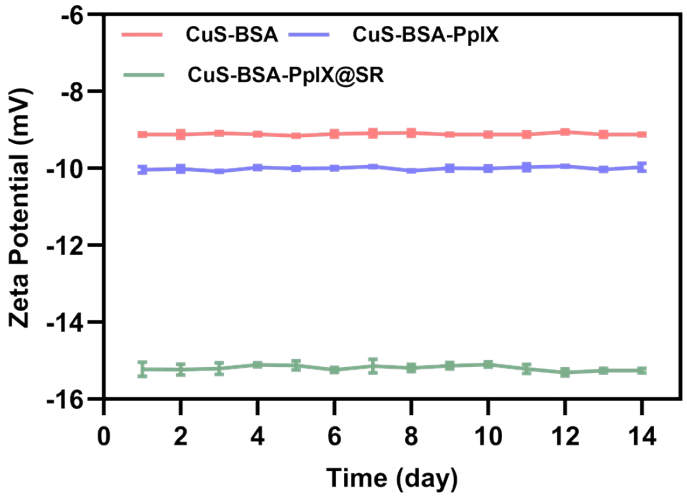

Figure S7. Zeta potential stability analysis of CuS-BSA, CuS-BSA-PpIX and CuS-BSA-PpIX@SR after incubation in PBS for 14 days. Data are presented as mean ± SD (n = 3).

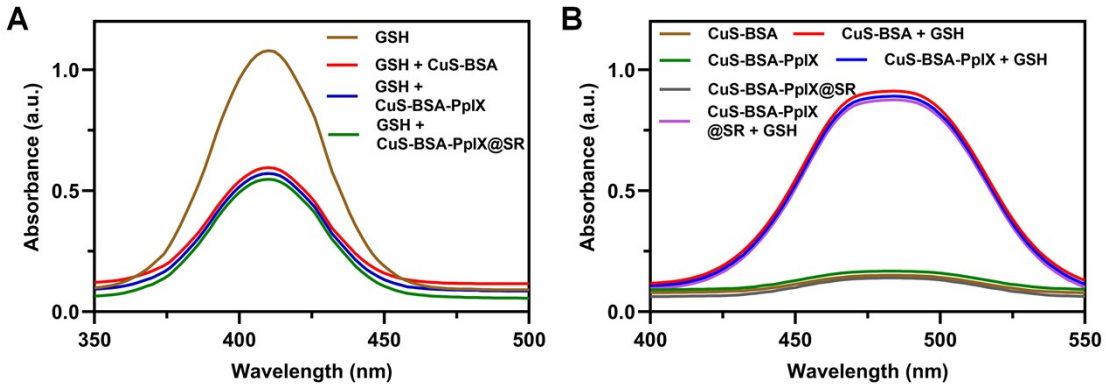

Figure S8. (A). UV-Vis of residual GSH after incubation with various CuS-based nanoplatforms. (B). UV-Vis of Cu^{+} generated by various CuS-based nanoplatforms in the presence of GSH.

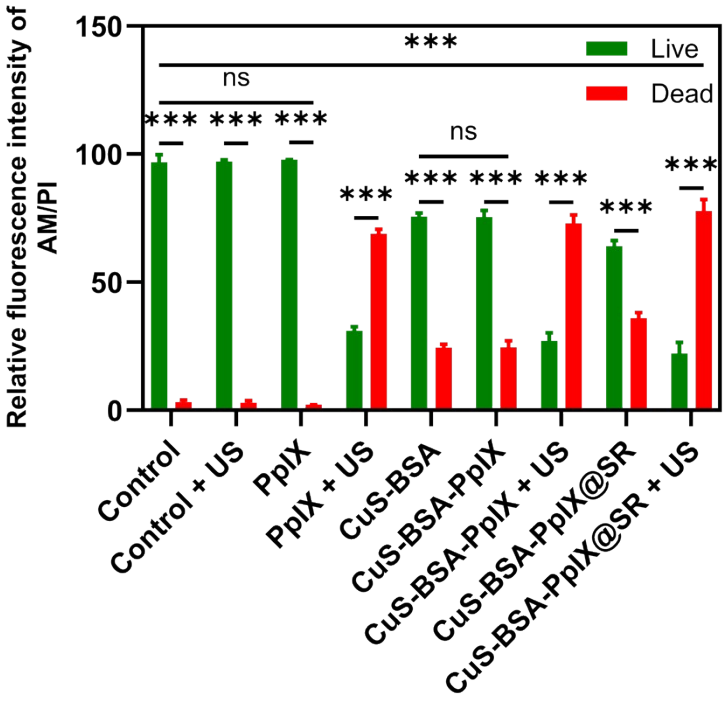

Figure S9. Semi-quantitative analysis of live (green) and dead (red) cell fluorescence intensity based on live/dead staining images. Data are presented as mean ± SD (n = 3). Statistical analysis was performed using two-way ANOVA.

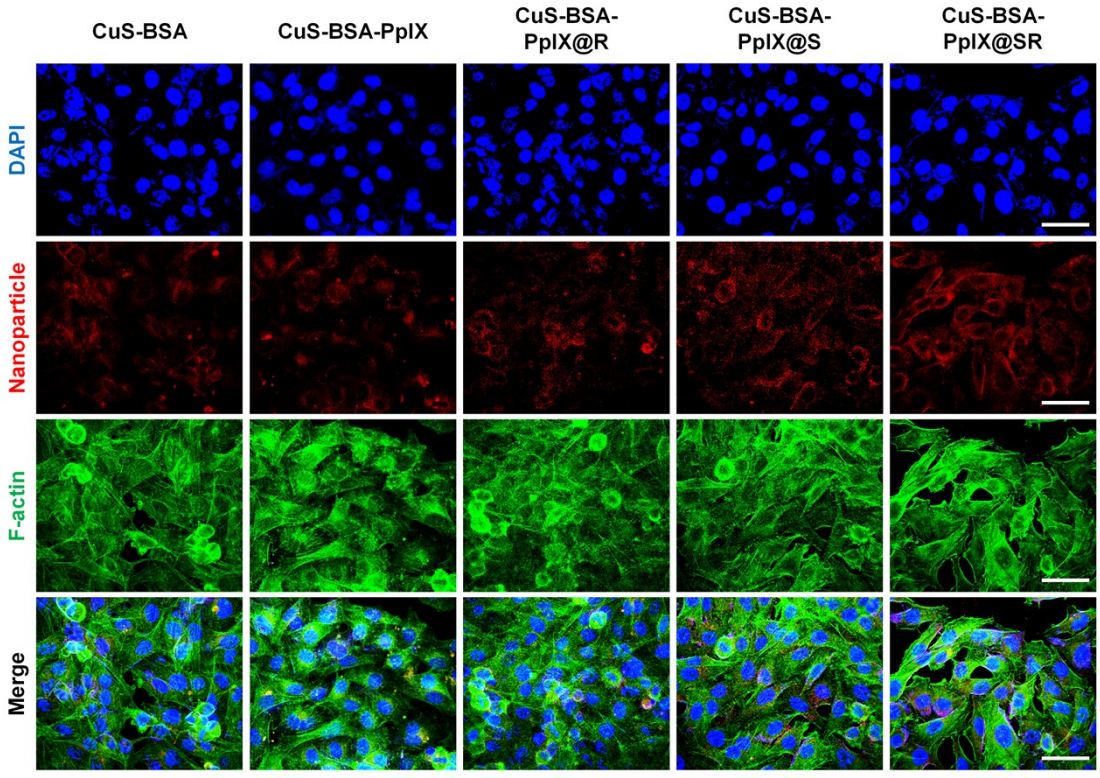

Figure S10. Confocal fluorescence images of HUVEC cells after nanoparticle treatment (scale bar: 50 μm).

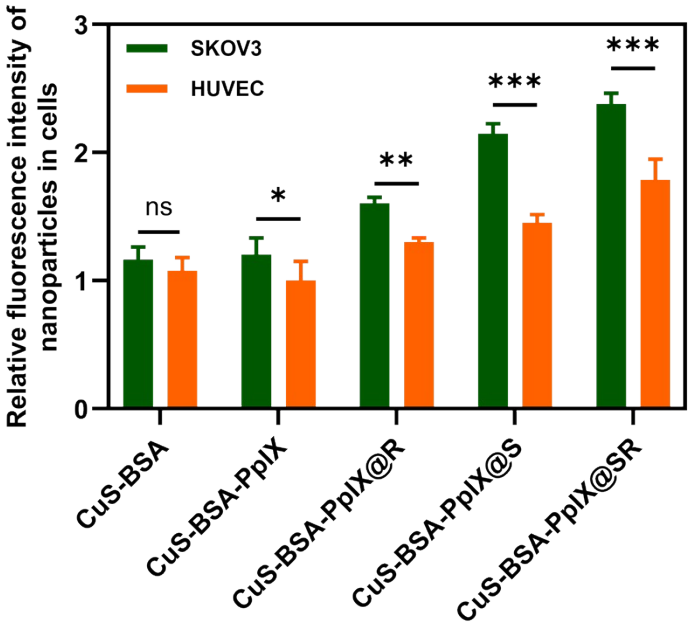

Figure S11. Semi-quantitative analysis of nanoparticle uptake by SKOV3 and HUVEC cells after co-incubation. Data are presented as mean ± SD (n = 3). Statistical analysis: two-way ANOVA, Tukey's multiple-comparisons test. Significance differences are indicated as ns and ***p<0.001, respectively.

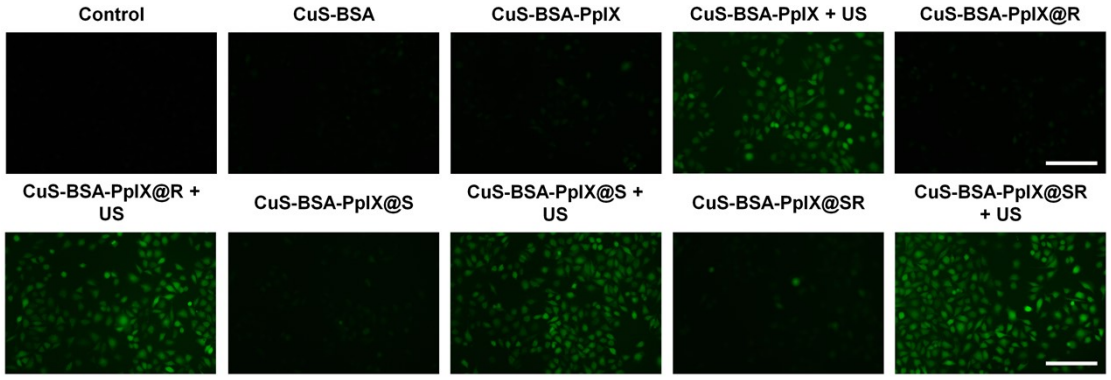

Figure S12. Detection of intracellular ROS generation in HUVEC cells after nanoparticle treatment (scale bar: 200 μm).

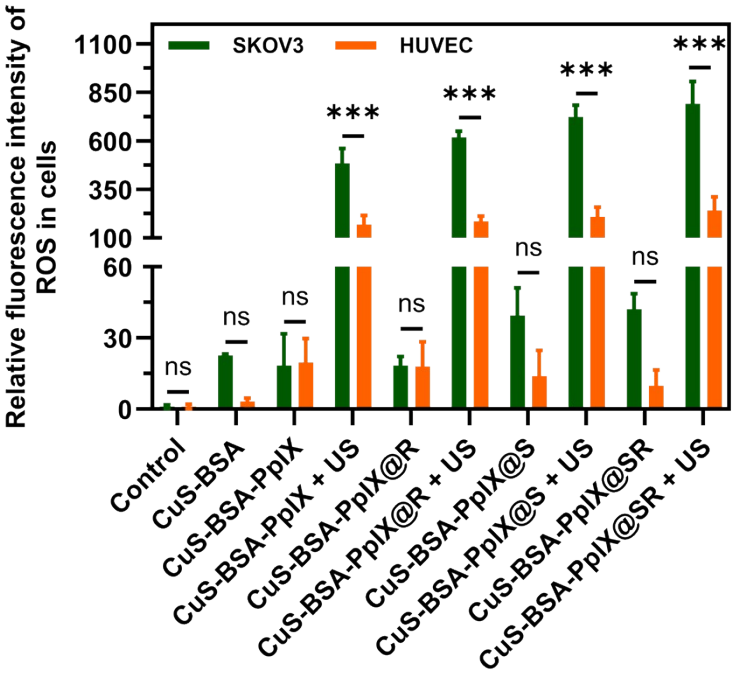

Figure S13. Semi-quantitative analysis of ROS generation by SKOV3 and HUVEC cells after co-incubation. Data are presented as mean ± SD (n = 3). Statistical analysis: two-way ANOVA, Tukey's multiple-comparisons test. Significance differences are indicated as ns, *p<0.05 and ***p<0.001, respectively.

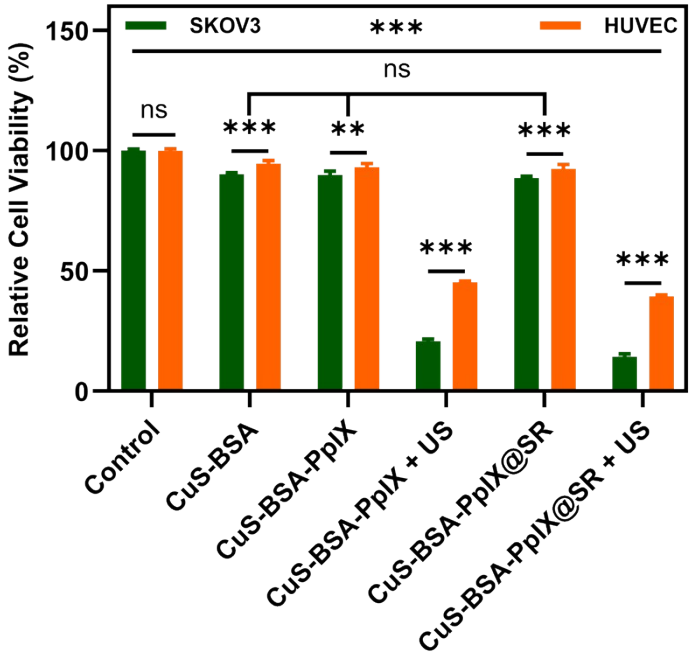

Figure S14. Comparison of cell viability after co-culture of nanoparticles with SKOV3 and HUVEC cells. Data are presented as mean ± SD (n = 3). Statistical analysis: two-way ANOVA, Tukey's multiple-comparisons test. Significance differences are indicated as ns, **p<0.01 and

***p<0.001, respectively.

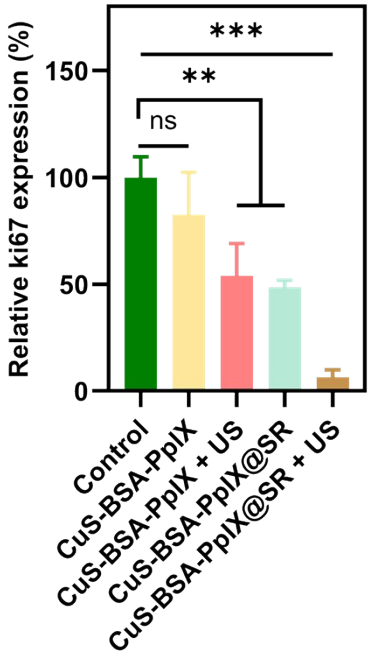

Figure S15. Semi-quantification of ki67-positive cells in tumor tissues. Data are presented as mean ± SD (n = 3). Statistical analysis: one-way ANOVA, Tukey's multiple-comparisons test. Significance differences are indicated as ns, **p<0.01 and ***p<0.001, respectively.

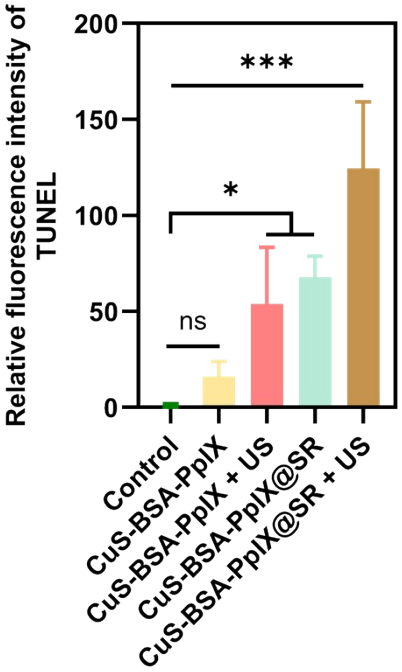

Figure S16. Semi-quantification of TUNEL-positive cells in tumor tissues. Data are presented as

mean ± SD (n = 3). Statistical analysis: one-way ANOVA, Tukey's multiple-comparisons test. Significance differences are indicated as ns, *p<0.05 and ***p<0.001, respectively.